Received April 21, 2022, accepted June 1, 2022, date of publication June 8, 2022, date of current version June 17, 2022.

Digital Object Identifier 10.1109/ACCESS.2022.3181195

Circuit Analysis of a Coplanar Waveguide (CPW) Terminated With a Step-Impedance Resonator (SIR) for Highly Sensitive One-Port Permittivity Sensing

PAU CASACUBERTA[1], PARIS VÉLEZ[1], (Senior Member, IEEE), JONATHAN MUÑOZ-ENANO[1], (Graduate Student Member, IEEE), LIJUAN SU[1], (Member, IEEE), MARTA GIL BARBA[2], (Member, IEEE), AMIR EBRAHIMI[3], (Member, IEEE), AND FERRAN MARTÍN[1], (Fellow, IEEE)

[1]GEMMA/CIMITEC, Departament d'Enginyeria Electrònica, Universitat Autònoma de Barcelona, 08193 Bellaterra, Spain
[2]Departamento Ingeniería Audiovisual y Comunicaciones, Universidad Politécnica de Madrid, 28031 Madrid, Spain
[3]School of Engineering, Royal Melbourne Institute of Technology (RMIT University), Melbourne, VIC 3001, Australia

Corresponding author: Pau Casacuberta (pau.casacuberta@uab.cat)

This work was supported in part by Ministerio de Ciencia e Innovación (MCIN)/Agencia Estatal de Investigación (AEI), Spain, through European Regional Development Fund (ERDF) European Union under Grant 10.13039/501100011033 and Grant PID2019-103904RB-I00; in part by the European Union Next Generation EU/PRTR under Grant PDC2021-121085-I00; and in part by the Agència de Gestió d'Ajuts Universitaris i de Recerca (AGAUR) Research Agency, Catalonia Government, under Project 2017SGR-1159. The work of Pau Casacuberta was supported by the Ministerio de Universidades, Spain, through the FPU (Ayudas para la Formación de Profesorado Universitario) under Grant FPU20/05700. The work of Jonathan Muñoz-enano was supported in part by the Secreteraria d'Universitats i Recerca (Gen. Cat.), and in part by the European Social Fund for the FI Grant. The work of Lijuan Su was supported by the Juan de la Cierva Program under Project IJC2019-040786-I. The work of Marta Gil Barba was supported in part by the Polytechnic University of Madrid, and in part by the Administration of the Community of Madrid through the V PRICIT Excellence Program for University Professoriate under Grant M190020074B. The work of Ferran Martín was supported by the Institució Catalana de Recerca i Estudis Avançats.

ABSTRACT This paper presents a single-frequency reflective-mode phase-variation microwave sensor devoted to the dielectric characterization of materials. The device is implemented in coplanar waveguide (CPW) technology and consists of two parts: (i) the sensing region, a step-impedance resonator (SIR) as termination of a CPW transmission line, and (ii) the design region, a cascade of high/low impedance quarter-wavelength inverters, used to boost up the sensitivity. By placing the so-called material under test (MUT) on top of the sensing region, the capacitance of the SIR is altered due to the effects of the dielectric constant of the MUT. This modifies the phase of the reflection coefficient seen from the input port, the output variable. From a circuit analysis, it is demonstrated that the sensitivity for small perturbations in the vicinity of the dielectric constant of a reference (REF) material can be optimized by setting the operation frequency of the sensor to the resonance frequency of the SIR loaded with such REF material. The maximum sensitivity in one of the reported sensors is as high as 66.5°, and the main figure of merit, defined as the ratio between the maximum sensitivity and the area of the sensing region expressed in terms of the squared guided wavelength, is FoM $= 3643°/\lambda^2$. Such figure of merit represents a significant improvement as compared to the one of the equivalent sensor implemented by means of an open-ended quarter-wavelength sensing line. Such equivalence between the semi-lumped element (i.e., SIR-based) sensor and the fully distributed counterpart is also analyzed in the paper.

INDEX TERMS Coplanar waveguide (CPW), dielectric characterization, microwave sensor, phase-variation sensor, permittivity sensor, reflective-mode sensor, step-impedance resonator (SIR).

I. INTRODUCTION

Material sensing using electrically small planar microwave resonators has experienced a significant growth in recent years. The reason is twofold: (i) microwaves are very

The associate editor coordinating the review of this manuscript and approving it for publication was Wen-Sheng Zhao.

sensitive to the materials to which they interact, and (ii) electrically small planar resonators are ideal sensing elements to implement devices with small sensing regions. Moreover, planar microwave resonators exhibit the inherent advantages of planar technology, including low cost and profile, potential implementation on flexible substrates (of interest, e.g., for the development of conformal sensors [1], [2] and wearable sensors [3]), compatibility with other technologies, such as microfluidics [4]–[11], or lab-on-a-chip [12], among others, and the possibility to integrate the associated electronics for post-processing and, eventually, for communication purposes in the same substrate.

Most planar microwave sensors based on resonant elements (either devoted to the dielectric characterization of materials or to the measurement of other parameters, e.g., space variables) exploit frequency variation [6], [13]–[20]. In particular, for material characterization, the resonance frequency of the sensing element is determined by the dielectric constant of the so-called material under test (MUT), provided it is located in the area of influence of the electromagnetic field generated by the sensing resonator. Additionally, the peak or notch magnitude of the resonance is influenced by the loss factor of the MUT. Therefore, it is possible to infer the complex dielectric constant of the MUT on the basis of the resonance frequency and magnitude variation measured, e.g., in a resonator-loaded line (the typical topology of frequency-variation sensors in planar configuration) [16], [19].

Frequency-variation sensors are robust against the effects of electromagnetic interference (EMI) and noise, but such sensors need wideband interrogation signals for measuring purposes, and this increases the cost of the associated electronics required for the generation of such signals, based on wideband voltage controlled oscillators (VCOs). This limitation applies also to the so-called frequency-splitting sensors [7], [21], [26], a variant of frequency-variation sensors where a host transmission line is loaded with a pair of identical resonant elements. In frequency-splitting sensors, similar to differential-mode sensors [8], [9], [27]–[36], one of the resonators acts as reference (REF) resonator, thereby accommodating the so-called reference (REF) material, whereas the MUT should be placed on top of the other resonant element. The working principle is based on the frequency splitting caused when the REF and MUT samples exhibit different properties. An advantage over frequency-variation sensors concerns the fact that, operating quasi-differentially, frequency-splitting sensors ''perceive'' the ambient factors, such as temperature and humidity, as common-mode stimuli, and therefore are robust against cross-sensitivities due to changes in environmental conditions.

Single-frequency sensors constitute a good solution to reduce the costs of the associated electronics. Among them, coupling-modulation sensors have been proposed [37]–[47]. In such sensors, a transmission line is symmetrically loaded with a single symmetric resonator, and the combination of both elements should prevent their mutual coupling. However, such coupling is activated when symmetry is truncated, e.g., by the effects of an asymmetric dielectric loading, or as consequence of a relative displacement (either linear or angular) between the sensing resonator and the host line (indeed, most coupling-modulation sensors are devoted to the measurement of space variables). In these sensors, the typical output variable is the magnitude of either a transmission coefficient or a voltage, and therefore coupling modulation sensors are less tolerant to effects of EMI and noise, at least as compared to frequency-variation and frequency splitting sensors.

Recently, a significant effort has been dedicated to the implementation of phase-variation sensors [27], [29], [33], [35], [36], [48]–[57], since these sensors combine the advantages of coupling-modulation sensors, i.e., operation at a single frequency, and frequency- variation/splitting sensors, as far as phase measurements are noise- and EMI-tolerant (nevertheless, in some realizations, the phase information was transformed to magnitude information [27], [35], [36]). Although examples of phase-variation sensors devoted to the measurement of space variables have been reported [54]–[56], the canonical application of these sensors is the measurement of the permittivity of the MUT, and other variables related to it, e.g., material composition, solute concentration in liquid mixtures, etc. Phase-variation sensors are also of interest for the identification of tiny defects in samples (based on the changes that such imperfections produce in the effective dielectric constant of the MUT), by virtue of the highly achievable sensitivity in such sensors [33], [36], [50].

Phase-variation permittivity sensors can be implemented by means of a transmission line, as far as the electrical length, or phase, of the line is subjected to the effects of the dielectric constant of the MUT, which should be placed on top of it [29], [33], [36]. Such electrical length, in turn, determines the phase of the transmission or reflection coefficient, the usual output variable. The sensitivity in these sensors, a key parameter, is proportional to the physical length of the line, provided the sensing region extends over the entire length of the line. For this reason, phase-variation sensors are typically implemented by means of meandered lines [33], [36]. An alternative strategy to optimize the sensitivity is to replace the ordinary (meandered) sensing line with highly-dispersive lines, e.g., composite right/left handed (CRLH) [27], electro-inductive-wave (EIW) [35], or slow-wave [52], [53] transmission lines. The sensitivity in the previous meander-line and artificial-line based sensors is good. It is especially remarkable that the CRLH- [27] and EIW-based [35] sensors exhibit very high sensitivity with a small sensing region. Nevertheless, the design of such sensors is not simple, and sensor performance is subjected to potential detuning effects of the involved resonators (eventually caused by fabrication related tolerances).

Recently, a different strategy for permittivity sensing, based on the measurement of the phase of the reflection coefficient in one-port structures, has been reported [48]–[51]. These reflective-mode sensors exhibit an unprecedentedly

high sensitivity with a small sensing area. The devices consist of an open-ended sensing line (either a half- or a quarter-wavelength line) cascaded to a set quarter-wavelength line sections with alternating high and low characteristic impedance (impedance inverters), and sensitivity optimization is based on the impedance contrast of the inverters and sensing line.

The figure of merit (FoM) of phase-variation sensors is the maximum sensitivity divided by the area of the sensing region expressed in terms of the guided wavelength at the operating frequency. Such FoM is high in these reflective-mode phase-variation sensors, since the sensing region is restricted only to the half- or quarter-wavelength open-ended sensing line. However, the FoM can be further optimized by replacing the open-ended sensing lines with semi-lumped planar resonators, providing a similar behavior, but with a substantially smaller size. This approach was first reported in [51], where an open complementary split ring resonator (OCSRR) [58], [59] is the sensing element that substitutes the half-wavelength open-ended sensing line of the fully distributed sensor. A significant improvement of the FoM was achieved by using the OCSRR sensing element [51].

Despite the very good sensor performance indicators reported in [51], the OCSRR is not exempt of certain design complexity. It behaves essentially as a parallel resonant tank (equivalent to an open-ended half-wavelength line at resonance), but it exhibits a series inductance and a parasitic shunt capacitance which are not easily controllable parameters, and should be taken into account for design purposes (specifically the parasitic capacitance, as discussed in [51]). Moreover, the sensors in [51] were implemented in coplanar waveguide (CPW) technology, thereby making necessary the use of vias and backside strips (with an equivalent functionality to air bridges) for the suppression of the parasitic slot mode (the OCSRR-terminated CPW does not exhibit axial symmetry).

In this paper, the main aim is to design and implement a reflective-mode phase-variation permittivity sensor in CPW technology, where the sensing element is a series step-impedance resonator (SIR), a symmetric semi-lumped resonator that can be described to a very good approximation by means of a series LC tank [60]–[62]. It is also an objective of the paper to demonstrate the equivalence between the proposed SIR-based sensor and the fully distributed counterpart, in this case based on a quarter-wavelength open-ended sensing line (also described by a series LC tank in the vicinity of resonance [63]). Design simplicity and the absence of vias are clear advantages over the sensor version based on OCSRRs, whilst the FoM is also very good, as it will be later demonstrated.

The paper is organized as follows. Section II presents the proposed SIR-based sensor, the working principle, and the circuit model. Moreover, this circuit model is validated in such section. A detailed circuit analysis of the equivalent circuit, focused on obtaining design guidelines for sensitivity optimization, is reported in Section III. The equivalence with the fully distributed sensor, based on a quarter-wavelength sensing line, is also included in Section III. In Section IV, several prototype sensors are designed, fabricated, and validated by means of electromagnetic simulation and experiment. Moreover, sensor performance is compared to the one of the distributed counterparts. A discussion relative to cross-sensitivities and effect of losses is carried out in Section V. Section VI is devoted to a comparison with other phase-variation sensors. Finally, Section VII concludes the work.

II. SENSOR TOPOLOGY, WORKING PRINCIPLE, AND CIRCUIT MODEL

It was demonstrated in [48] that highly sensitive phase-variation permittivity sensors can be implemented by means of either a quarter- or a half-wavelength open-ended sensing line cascaded to a set of quarter-wavelength transmission line sections with alternating high and low characteristic impedance (impedance inverters), as compared to the reference impedance of the ports (typically 50 Ω). Fig. 1(a) depicts a typical topology by considering sensor implementation in CPW technology, and a quarter-wavelength sensing line. By placing a certain MUT on top of the sensitive region (indicated with a dashed rectangle in Fig. 1), the phase of such line is modified, due to the change in the effective dielectric constant of the line, determined by the dielectric constant of the MUT, $\varepsilon_{\mathrm{MUT}}$. This variation in the phase of the sensing line in turn modifies the phase of the reflection coefficient, the output variable. Thus, the sensitivity, a key parameter, is defined as the derivative of the phase of the reflection coefficient with the dielectric constant of the MUT, the input variable.

For sensitivity optimization, the sensing line should exhibit a high characteristic impedance provided its length is a quarter-wavelength (or an odd multiple) at the operating frequency [48]. Contrarily, for half-wavelength (or multiples of this length) open-ended sensing lines, the impedance should be set to a low value in order to enhance the sensitivity. Moreover, the impedance inverters must exhibit an alternating high and low impedance, but it is necessary that the inverter adjacent to the sensing line exhibits a high impedance for low-impedance half-wavelength open-ended sensing lines, and a low impedance when the sensing line is a quarter-wavelength high-impedance line (the situation corresponding to the topology of Fig. 1). This set of inverters generates a multiplicative effect on the sensitivity, intimately related to the square of the impedance contrast of the different line sections, as reported in [48]. The resulting sensors, thereby, exhibit an unprecedentedly high sensitivity.

Fig. 1(b) depicts the circuit schematic, where the electrical parameters (i.e., the characteristic impedance and the phase, or electrical length) of the different line sections are indicated. The sub-index s is used to designate the parameters in reference to the sensing line, Z_s being the impedance and ϕ_s the phase of this line. The impedance and phase of the high/low impedance line sections are differentiated by the numerical sub-index i, with $i = 1, \ldots N$, where N is the

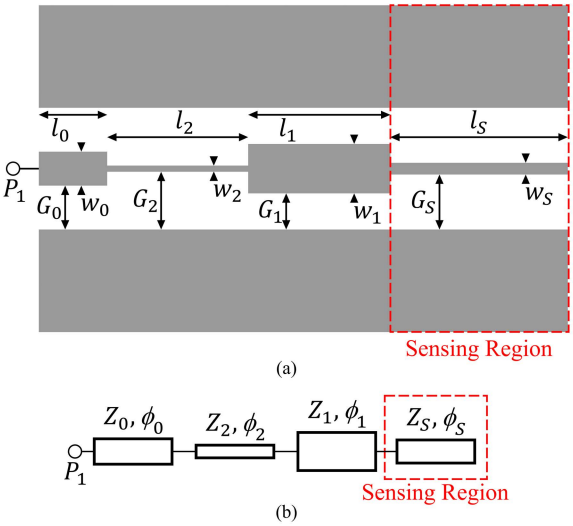

FIGURE 1. Typical topology (a), in CPW technology, and circuit schematic (b) of the one-port reflective-mode phase-variation sensor based on a set of high/low impedance quarter-wavelength impedance inverters and a quarter-wavelength open-ended sensing line. The sensing region is indicated with a dashed rectangle. For the topology, a pair ($N = 2$) of high/low impedance 90° line sections are considered. The electrical and geometrical variables are indicated.

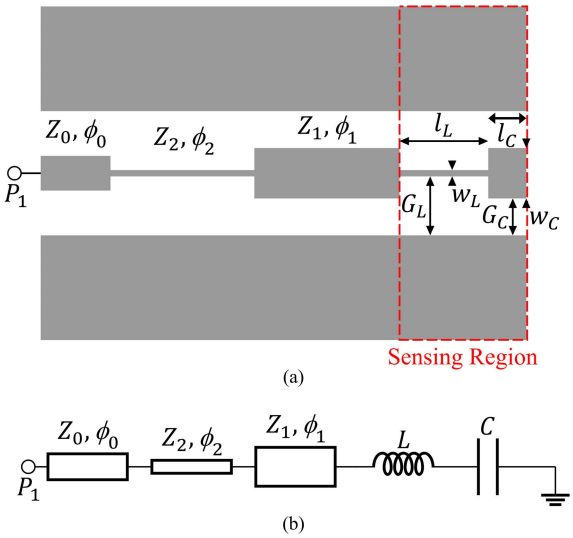

FIGURE 2. Typical topology (a) and circuit schematic (b) of the one-port reflective-mode phase-variation permittivity sensor identical to the one of Fig. 1, with the quarter-wavelength sensing line replaced with a SIR resonator (the sensing element). The sensing region is indicated with a dashed rectangle. The relevant dimension variables of the SIR are indicated (the dimensions of the high/low impedance 90° lines are designated by the same variables as in Fig. 1). For the simulations referred to in the text, the dimensions of the SIR (in mm) are: $w_L = 0.20$, $G_L = 0.90$, $l_L = 7.33$, $w_C = 1.60$, $G_C = 0.20$, $l_C = 3.04$.

number of inverters. Finally, the access line, with impedance Z_0, identical to the reference impedance of the port, has a phase designated as ϕ_0.

The sensors subject of the present work are based on the same principle. The difference with regard to the sensor depicted in Fig. 1 concerns the sensitive region, consisting in a step-impedance resonator (SIR), rather than a quarter-wavelength open-ended line section. With such SIR termination of the line, a substantially smaller sensing region is envisaged, by virtue of the small electrical size of the SIR, a semi-lumped resonator. Moreover, this reduction in the sensing region can be achieved by maintaining the same maximum sensitivity, as it will be later demonstrated. Thus, a substantially improved figure of merit (FoM), or ratio between the maximum sensitivity and the area of the sensing region, is expected in these new SIR-based phase-variation permittivity sensors, as compared to the FoM of the fully distributed counterparts. This improved FoM is important in applications requiring high sensitivity combined with small MUT samples, for example, to monitor tiny variations in the composition of liquid samples (for that purpose, adding a fluidic channel on top of the sensing region is an option, but submersible sensors [64] are also possible).

The topology and circuit schematic of these SIR-terminated CPW sensors are depicted in Fig. 2, where the same geometrical and electrical variables describing the quarter-wavelength inverters of the sensor of Fig. 1 are used. The SIR is modelled by means of a grounded series resonator, with inductance L and capacitance C [62].

For validation of the SIR-terminated CPW, we will consider the structure of Fig. 2, but excluding the high/low impedance quarter-wavelength line sections and access lines (the dimensions are indicated in the caption). The phase response of this one-port structure is depicted in Fig. 3. It has been inferred by means of the *Keysight ADS* electromagnetic simulator, and the considered substrate is the *Rogers RO3010* with dielectric constant $\varepsilon_r = 10.2$ and thickness $h = 1.27$ mm (losses are excluded in the simulation). For low frequencies the structure exhibits a capacitive behavior, and the input impedance is an open-circuit in the DC limit (the phase of the reflection coefficient is $\phi_\rho = 0°$ in that limit). At the SIR resonance frequency, given by

$$f_0 = \frac{1}{2\pi\sqrt{LC}} \tag{1}$$

the impedance seen from the input port is null. This frequency can be inferred from the discontinuity in the phase response, where the phase satisfies $\phi_\rho = \pm 180°$, corresponding to a short-circuit. Above resonance, the SIR exhibits a positive (inductive) reactance, and, as frequency increases, the phase of the reflection coefficient progressively approaches $\phi_\rho = 0°$. To univocally determine the two reactive parameters of the SIR, an additional condition is needed. Such condition is the phase slope at resonance, given by

$$\left.\frac{d\phi_\rho}{d\omega}\right|_{\omega_0} = -\frac{4L}{Z_0} \tag{2}$$

where $\omega_0 = 2\pi f_0$ is the angular resonance frequency. With (1) and (2), L and C can be easily inferred from the frequency dependence of the phase of the reflection coefficient. The values for the structure of Fig. 2 are found to be $L = 4.375$ nH and $C = 1.164$ pF. The phase of the reflection coefficient that corresponds to an LC series resonator with such element values is also depicted in Fig. 3. The agreement with the phase inferred form electromagnetic simulation is very good,

thereby, these results point out the validity of the model and the parameter extraction method.

Let us now consider that the sensitive region is covered by a semi-infinite (in the vertical direction) MUT, so that the electromagnetic field generated in the SIR does not reach the MUT/air interface. If we also assume that the substrate can be considered to be semi-infinite, the capacitance of the MUT-loaded SIR, C', can be expressed in terms of the capacitance of the bare SIR as follows [51]

$$C' = C\frac{\varepsilon_r + \varepsilon_{\rm MUT}}{\varepsilon_r + 1} \tag{3a}$$

where ε_r is the substrate dielectric constant. This assumption was adopted in [51]. However, it was demonstrated in [65] that by introducing the concept of equivalent dielectric constant of the substrate, $\varepsilon_{r,\rm eq}$, defined as the dielectric constant of a hypothetical semi-infinite substrate providing the same contribution to the capacitance of the resonant element, the total capacitance of the MUT-loaded SIR, C', can be expressed as

$$C' = C\frac{\varepsilon_{r,\rm eq} + \varepsilon_{\rm MUT}}{\varepsilon_{r,\rm eq} + 1} \tag{3b}$$

providing a more accurate prediction. The equivalent dielectric constant of the considered substrate (*Rogers RO3010* with dielectric constant $\varepsilon_r = 10.2$ and thickness $h = 1.27$ mm) was determined by the method described in [65], based on electromagnetic simulations (using *ANSYS HFSS* software). The value was found to be $\varepsilon_{r,\rm eq} = 9.48$, i.e., somehow smaller than ε_r, the nominal dielectric constant of the substrate.

To validate expression (3b), the phase responses of the SIR-terminated CPW covered with several hypothetical semi-infinite MUT samples, with different value of $\varepsilon_{\rm MUT}$, have been obtained by electromagnetic simulation. As expected (the responses are also included in Fig. 3), as $\varepsilon_{\rm MUT}$ increases, the capacitance C' increases, and the resonance of the SIR decreases. Fig. 3 also depicts the phase responses inferred from circuit simulation of the series resonators described by an identical inductance, namely, L (the one extracted from the response of the bare SIR), and capacitances given by (3b) for the different values of $\varepsilon_{\rm MUT}$ (such capacitances are indicated in Fig. 3). As it can be seen, the agreement with the electromagnetically simulated phases is excellent. Moreover, the capacitances C' deduced from the resonance frequencies corresponding to the different electromagnetic simulations, indicated in the caption of Fig. 3, are roughly identical to those given by (3b). These results validate the circuit model of the MUT-loaded SIR-terminated CPW with capacitance given by expression (3b), under the mentioned semi-infinite MUT approximation.

III. CIRCUIT ANALYSIS FOR SENSITIVITY OPTIMIZATION

The proposed sensors (Fig. 2) can potentially exhibit an unprecedentedly high sensitivity by adequately choosing the operating frequency, the SIR quality factor, as well as the

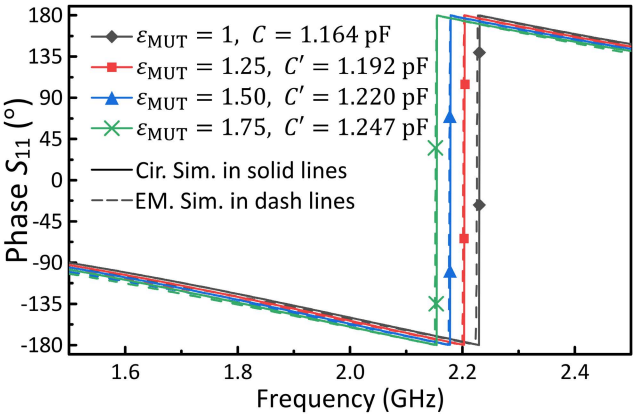

FIGURE 3. Phase of the reflection coefficient of the SIR-terminated CPW structure of Fig. 2, excluding the cascaded high/low impedance quarter-wavelength impedance inverters and access lines. The different curves correspond to the uncovered SIR (with capacitance $C = 1.164$ pF), and to the SIR covered with various semi-infinite MUTs with the indicated dielectric constant and capacitance C'. The SIR inductance in all the cases is $L = 4.375$ nH. The capacitances for the different considered MUTs obtained from the resonance frequency of the SIR, where the phase experiences a 180° jump, are $C' = 1.195$ pF (for $\varepsilon_{\rm MUT} = 1.25$), $C' = 1.223$ pF (for $\varepsilon_{\rm MUT} = 1.50$), and $C' = 1.250$ pF (for $\varepsilon_{\rm MUT} = 1.75$).

impedances of the quarter-wavelength impedance inverters. However, by increasing the sensitivity, the linearity is necessarily degraded [48]. Thus, the sensitivity of the sensor should be optimized in the vicinity of a certain value of the dielectric constant of the MUT. Such dielectric constant is designated as $\varepsilon_{\rm REF}$, and it is set to $\varepsilon_{\rm REF} = 3.55$ in this work, corresponding to the dielectric constant of one of the substrates available in our laboratory. This means that the intended sensors will be able to detect tiny variations of the dielectric constant of the MUT in the vicinity of $\varepsilon_{\rm REF}$, where the sensitivity is going to be optimized.

In order to obtain design guidelines for sensitivity optimization, and to predict the value of the maximum sensitivity, let us consider the circuit model of Fig. 2(b). However, let us first analyze only the SIR-terminated CPW structure. Then, the generalization to the whole device, with an arbitrary number of quarter-wavelength impedance inverters, will be carried out. Finally, the analysis of the equivalent sensor, based on a quarter-wavelength open-ended sensing line, will be reported, and the conditions to obtain the same sensitivity will be provided.

A. SIR-TERMINATED CPW

Let us designate by $Z_{\rm in}$ the impedance seen from the input port of the SIR-terminated CPW transmission line. The reflection coefficient seen from this port, with reference impedance Z_0, is given by [63]

$$\rho = \frac{Z_{\rm in} - Z_0}{Z_{\rm in} + Z_0} = \frac{j\chi_{\rm in} - Z_0}{j\chi_{\rm in} + Z_0} \tag{4}$$

where $\chi_{\rm in}$ is the input reactance. From (4), the phase of the reflection coefficient, the output variable, is simply

$$\phi_\rho = 2\arctan\left(-\frac{\chi_{\rm in}}{Z_0}\right) + \pi \tag{5}$$

Such phase is influenced by the input variable, $\varepsilon_{\mathrm{MUT}}$, through the effects of it on the SIR capacitance (see expression 3b), which, in turn, determines the input reactance of the SIR-terminated CPW, χ_{in}. The sensitivity can therefore be expressed as

$$S = \frac{d\phi_\rho}{d\varepsilon_{\mathrm{MUT}}} = \frac{d\phi_\rho}{dC'} \cdot \frac{dC'}{d\varepsilon_{\mathrm{MUT}}} \tag{6}$$

Let us call C'_{REF} the capacitance of the SIR when it is loaded with the REF material, given by (3b) with $\varepsilon_{\mathrm{MUT}} = \varepsilon_{\mathrm{REF}}$. Using (3b), the capacitance of the SIR loaded with an arbitrary MUT can be expressed in terms of C'_{REF} as

$$C' = C'_{\mathrm{REF}} \frac{\varepsilon_{r,\mathrm{eq}} + \varepsilon_{\mathrm{MUT}}}{\varepsilon_{r,\mathrm{eq}} + \varepsilon_{\mathrm{REF}}} \tag{7}$$

The capacitance C'_{REF} is a constant, and the capacitance of the MUT-loaded SIR can be expressed as $C' = C'_{\mathrm{REF}} + \Delta C$, with $\Delta C = 0$ for $\varepsilon_{\mathrm{MUT}} = \varepsilon_{\mathrm{REF}}$. Thus, expression (6) can be rewritten as

$$S = \frac{d\phi_\rho}{d\Delta C} \cdot \frac{d\Delta C}{d\varepsilon_{\mathrm{MUT}}} \tag{8}$$

Let us now express the reactance of the SIR-terminated CPW in terms of the resonance frequency of the SIR loaded with the reference material ($\omega_{0,\mathrm{REF}} = 1/\sqrt{LC'_{\mathrm{REF}}}$). The following result is obtained

$$\chi_{\mathrm{in}} = \omega L \left[1 - \frac{\omega_{0,\mathrm{REF}}^2}{\omega^2 \left(1 + \frac{\Delta C}{C'_{\mathrm{REF}}} \right)} \right] \tag{9}$$

and, from it, the phase of the reflection coefficient is simply

$$\phi_\rho = 2 \arctan \left\{ \frac{\omega L}{Z_0} \left[\frac{\omega_{0,\mathrm{REF}}^2}{\omega^2 \left(1 + \frac{\Delta C}{C'_{\mathrm{REF}}} \right)} - 1 \right] \right\} + \pi \tag{10}$$

The first term of the sensitivity, $d\phi_\rho/d\Delta C$, can be calculated from (10) and is found to be

$$\frac{d\phi_\rho}{d\Delta C} = \frac{-2}{1 + \frac{\chi_{\mathrm{in}}^2}{Z_0^2}} \cdot \frac{L\omega_{0,\mathrm{REF}}^2}{Z_0 \omega} \cdot \frac{1/C'_{\mathrm{REF}}}{\left[1 + \frac{\Delta C}{C'_{\mathrm{REF}}} \right]^2} \tag{11}$$

and such term in the limit of small perturbations of the dielectric constant of the MUT in the vicinity of $\varepsilon_{\mathrm{MUT}} = \varepsilon_{\mathrm{REF}}$ (or $\Delta C = 0$) is

$$\left. \frac{d\phi_\rho}{d\Delta C} \right|_{\Delta C = 0} \equiv S_{\Delta C}|_{\Delta C = 0} = \frac{-2Z_0 L \omega_{0,\mathrm{REF}}^2 / C'_{\mathrm{REF}} \omega}{Z_0^2 + L^2 \omega^2 \left(\frac{\omega_{0,\mathrm{REF}}^2}{\omega^2} - 1 \right)^2} \tag{12}$$

The second term contributing to the sensitivity is simply

$$\frac{d\Delta C}{d\varepsilon_{\mathrm{MUT}}} = \frac{C'_{\mathrm{REF}}}{\varepsilon_{r,\mathrm{eq}} + \varepsilon_{\mathrm{REF}}} \tag{13}$$

This term, neither depends on the operating frequency, nor on the dielectric constant of the MUT, contrary to the first term. Thus, for sensitivity optimization in the vicinity of the dielectric constant of the REF material $\varepsilon_{\mathrm{REF}}$, it is necessary to identify the operation frequency that maximizes expression (12). For that purpose, the derivative of (12) with frequency is obtained, and the corresponding result is forced to be null. The resulting equation is found to be

$$3 \frac{\omega^4}{\omega_{0,\mathrm{REF}}^4} - \left(2 - \frac{\omega'^2_0}{\omega_{0,\mathrm{REF}}^2} \right) \frac{\omega^2}{\omega_{0,\mathrm{REF}}^2} - 1 = 0 \tag{14}$$

where the following frequency variable has been defined in order to simplify the notation

$$\omega'^2_0 = \frac{Z_0^2}{L^2} \tag{15}$$

The solution of (14) is

$$\frac{\omega^2}{\omega_{0,\mathrm{REF}}^2} = \frac{1}{3} - \frac{1}{6} \frac{\omega'^2_0}{\omega_{0,\mathrm{REF}}^2} + \frac{2}{3} \sqrt{1 + \frac{1}{4} \left(\frac{1}{4} \frac{\omega'^4_0}{\omega_{0,\mathrm{REF}}^4} - \frac{\omega'^2_0}{\omega_{0,\mathrm{REF}}^2} \right)} \tag{16}$$

From this solution, it follows that if $\omega'^2_0/\omega_{0,\mathrm{REF}}^2 << 1$, the optimum frequency for sensitivity enhancement in the limit of small perturbations is roughly $\omega \approx \omega_{0,\mathrm{REF}}$, the resonance frequency of the SIR loaded with the REF sample. This condition is equivalent to

$$\frac{\omega'^2_0}{\omega_{0,\mathrm{REF}}^2} = Z_0^2 \frac{C'_{\mathrm{REF}}}{L} = \frac{16}{\pi^2} \frac{Z_0^2}{Z_s^2} \ll 1 \tag{17}$$

and can be fulfilled if the SIR exhibits a high inductance and a low capacitance. In (17), the equivalent impedance of the SIR resonator, defined as (see Appendix)

$$Z_s = \frac{4}{\pi} \sqrt{\frac{L}{C'_{\mathrm{REF}}}} \tag{18}$$

has been used.

Let us suppose that the SIR loaded with the REF material exhibits reactive elements satisfying the above condition (17). Introducing (12) and (13) in (8), the sensitivity in the limit of small perturbations (i.e., evaluated at $\varepsilon_{\mathrm{MUT}} = \varepsilon_{\mathrm{REF}}$, or $\Delta C = 0$) for the operating frequency set to $\omega \approx \omega_{0,\mathrm{REF}}$ is found to be

$$\begin{aligned} S|_{\Delta C = 0, \omega_{0,\mathrm{REF}}} &\equiv \left. \frac{d\phi_\rho}{d\varepsilon_{\mathrm{MUT}}} \right|_{\Delta C = 0, \omega_{0,\mathrm{REF}}} \\ &= -\frac{2\omega_{0,\mathrm{REF}} L}{Z_0(\varepsilon_{r,\mathrm{eq}} + \varepsilon_{\mathrm{REF}})} \end{aligned} \tag{19}$$

According to (19), sensitivity optimization requires a high value of L, and, consequently, a low value of C'_{REF}, so that the product of these reactive elements is coherent with the frequency of operation $\omega_{0,\mathrm{REF}} = 2\pi f_{0,\mathrm{REF}} = 1/\sqrt{LC'_{\mathrm{REF}}}$, in agreement with the condition (17). Therefore, in order to enhance the sensitivity at small perturbations, the equivalent impedance of the SIR, Z_s, must be high, and the frequency of operation must be set to $\omega_{0,\mathrm{REF}}$.

To gain more insight on the validity of condition (17), we have considered a SIR-terminated CPW identical to the

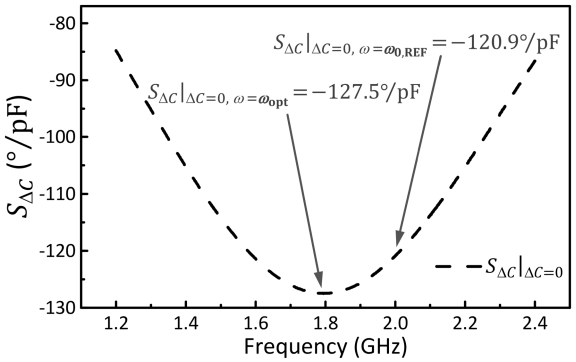

FIGURE 4. Dependence of the sensitivity in the limit of small perturbations with frequency, as given by (12). The value of maximum sensitivity alongside the one evaluated at the resonance frequency of the SIR is indicated.

one of Fig. 2, and a REF material with the dielectric constant indicated before ($\varepsilon_{\mathrm{REF}} = 3.55$). The reactive elements of the SIR loaded with such REF material are $L = 4.375$ nH and $C'_{\mathrm{REF}} = 1.447$ pF, and evaluation of (17) with $Z_0 = 50\ \Omega$ gives $\omega'^2_0/\omega^2_{0,\mathrm{REF}} = 0.827 < 1$. The exact solution of (14) gives $\omega^2/\omega^2_{0,\mathrm{REF}} = 0.805$, which means that the optimum frequency is very close to $\omega_{0,\mathrm{REF}}$ (i.e., $\omega_{\mathrm{opt}} = 0.897\omega_{0,\mathrm{REF}}$). Fig. 4 depicts the sensitivity at small perturbations as a function of frequency, as given by (12), for the above-cited reactive values of the SIR resonator. As expected, the maximum (absolute value) is located at ω_{opt}, where the sensitivity is found to be $S|_{\Delta C=0} = -127.5°/\mathrm{pF}$, slightly above the sensitivity at $\omega_{0,\mathrm{REF}}$, given by (19), i.e., $S|_{\Delta C=0,\ \omega_{0,\mathrm{REF}}} = -120.9°/\mathrm{pF}$. Nevertheless, in practice, tuning the operating frequency exactly to ω_{opt} is difficult due to fabrication related tolerances. If $\omega_{0,\mathrm{REF}}$ is similar to ω_{opt}, targeting the operating frequency at $\omega_{0,\mathrm{REF}}$ is reasonable, since this is an easily identifiable frequency. Moreover, any potential loss of sensitivity due to deviations regarding this value, or to the optimum frequency, can be compensated with the quarter-wavelength high/low impedance line sections, to be discussed next.

B. GENERALIZATION TO A SIR-TERMINATED STEP-IMPEDANCE CPW

In this subsection, the objective is to demonstrate that by cascading 90° line sections with alternating high and low characteristic impedance to the SIR-terminated CPW, the sensitivity can be further, and substantially, enhanced. Indeed, a similar behavior to the one of reflective-mode phase-variation dielectric constant sensors based on an open-ended 90° sensing line cascaded to a set of high/low impedance 90° line sections is expected [48]. The reason is that an open-ended 90° (sensing) line, like the SIR, can be described to a good approximation by a series resonator in the vicinity of resonance (see Appendix).

Let us consider the structure of Fig. 2 generalized to an arbitrary number, N, of 90° high/low impedance line sections. The impedance seen from the input port can be expressed as

$$Z_{\mathrm{in},N} = Z_{\mathrm{in}}^{(-1)^N} \cdot \prod_{i=1}^{N} \left\{ Z_i^{2\cdot(-1)^{i+N}} \right\} \tag{20}$$

where Z_i is the characteristic impedance of line section i (with $i = 1, 2, \ldots N$), and Π denotes the product operator. The reflection coefficient can thus be expressed as

$$\rho = \frac{j\,(-1)^N \cdot \chi_{\mathrm{in}}{}^{(-1)^N} \cdot \prod_{i=1}^{N} \left\{ Z_i^{2\cdot(-1)^{i+N}} \right\} - Z_0}{j\,(-1)^N \cdot \chi_{\mathrm{in}}{}^{(-1)^N} \cdot \prod_{i=1}^{N} \left\{ Z_i^{2\cdot(-1)^{i+N}} \right\} + Z_0} \tag{21}$$

and the phase of the reflection coefficient is

$$\phi_\rho = 2\arctan\left(-\frac{\chi_{\mathrm{in}}}{\dfrac{Z_0}{\prod_{i=1}^{N} \left\{ Z_i^{2\cdot(-1)^{i+N}} \right\}}} \right) + \pi \tag{22a}$$

for N even, and

$$\phi_\rho = 2\arctan\left(-\frac{\chi_{\mathrm{in}}}{\dfrac{\prod_{i=1}^{N} \left\{ Z_i^{2\cdot(-1)^{i+N}} \right\}}{Z_0}} \right) \tag{22b}$$

for N odd. The phases given by (22) and (5) are formally identical. The single difference concerns the denominator of the argument of the arctan, which is simply Z_0 in (5), and it exhibits a quadratic dependence with the impedances, Z_i, of the different 90° line sections in (22). Thus, the sensitivity for the SIR-terminated structure with cascaded high/low impedance 90° line sections is given by expression (19) by replacing Z_0 with the denominators of expressions (22). The following results are obtained for N even and odd, respectively

$$S|_{\Delta C=0,\omega_0} = -\frac{2\omega_{0,\mathrm{REF}}L}{(\varepsilon_{r,\mathrm{eq}}+1)} \cdot \frac{\prod_{i=1}^{N} \left\{ Z_i^{2\cdot(-1)^{i+N}} \right\}}{Z_0} \quad (N \text{ even}) \tag{23a}$$

$$S|_{\Delta C=0,\omega_0} = -\frac{2\omega_{0,\mathrm{REF}}L}{(\varepsilon_{r,\mathrm{eq}}+1)} \cdot \frac{Z_0}{\prod_{i=1}^{N} \left\{ Z_i^{2\cdot(-1)^{i+N}} \right\}} \quad (N \text{ odd}) \tag{23b}$$

It is clear from (23) that if the impedances of the 90° line sections with odd index are set to low values, as compared to Z_0, and those corresponding to line sections with even index are high, the resulting sensitivity is substantially higher than the one given by (19). The reason is that there is a multiplicative effect that depends on the square of the normalized impedances of the different line sections, with the odd-index (low) impedances and the even-index (high) impedances appearing in the denominator and numerator of (23), respectively. The limit in the achievable multiplication factor (second term in the product of expressions 23) is dictated by the maximum and minimum achievable values of the CPW line impedance. Nevertheless, the sensitivity in the limit of small perturbations can be unprecedentedly increased to the desired value by simply adding the necessary 90° high/low impedance line sections. Obviously, this penalizes

the overall sensor size, but not the sensitive region, circumscribed to the area occupied by the SIR resonator (the sensing element). As it will be shown, sensitivity enhancement in the limit of small perturbations also degrades the linearity of the sensor. However, such sensitivity enhancement is of special interest for the implementation of highly sensitive devices, able to resolve small variations in the dielectric constant of the MUT in the vicinity of that of the REF material (if measurements over a wide input dynamic range are pursuit, in that case, a moderate sensor sensitivity in favor of better linearity might be preferred).

It is worth mentioning that, recently, several strategies to enhance the sensitivity in frequency variation sensors, with very competitive results, have been reported, including metamaterial coupling [66], intermodulation products using active resonators [67], and coupled resonators [68].

C. COMPARISON TO THE EQUIVALENT SENSOR BASED ON A QUARTER-WAVELENGTH OPEN-ENDED SENSING LINE

By virtue of the analogy between a 90° open-ended line and a series resonator in the vicinity of resonance (see Appendix), a similar behavior between the proposed SIR-based sensors and those reported in [48], where the sensing structure is a quarter-wavelength open-ended line, is expected. Let us next demonstrate the equivalence between the sensitivity in both sensor types.

By excluding the high/low impedance 90° line sections, the sensitivity of the quarter-wavelength based sensor in the vicinity of the dielectric constant of the REF sample is [48]

$$\frac{d\phi_\rho}{d\varepsilon_{\text{MUT}}} = -2\frac{Z_s}{Z_0}\cdot\frac{\omega_{0,\text{REF}}l_s}{2\sqrt{2}c}\cdot\frac{1}{\sqrt{\varepsilon_{r,\text{eq}}+\varepsilon_{\text{REF}}}} \tag{24}$$

where l_s and Z_s are the length and characteristic impedance, respectively, of the 90° open-ended sensing line, $\omega_{0,\text{REF}}$ is the operating frequency (providing the required 90° electrical length to the sensing line covered with the REF sample), and c is the speed of light in vacuum. Since the phase of the line at ω_0 is

$$\phi_s = \frac{\pi}{2} = \frac{\omega_{0,\text{REF}}l_s}{v_p}, \tag{25}$$

v_p being the phase velocity

$$v_p = \frac{c}{\sqrt{\varepsilon_{\text{eff}}}}, \tag{26}$$

with the effective dielectric constant of a CPW given by

$$\varepsilon_{\text{eff}} = \frac{\varepsilon_{r,\text{eq}}+\varepsilon_{\text{REF}}}{2}, \tag{27}$$

it follows that (24) can be rewritten as

$$\frac{d\phi_\rho}{d\varepsilon_{\text{MUT}}} = -\frac{Z_s}{2Z_0}\cdot\frac{\pi}{\varepsilon_{r,\text{eq}}+\varepsilon_{\text{REF}}} \tag{28}$$

Let us now use the equivalent impedance of the SIR resonator as defined in (18). By introducing it in (28), the sensitivity is found to be identical to the one of the SIR-based sensor in the limit of small perturbations, and given by (19). By including a certain set of high/low impedance 90° line sections (for sensitivity enhancement), the sensitivities of both the SIR-based sensor and the fully distributed counterpart (based on a 90° sensing line) are also identical and given by expressions (23), provided the mapping of (18) is fulfilled. It should be emphasized that these identical sensitivities between both sensing structures take place in the limit of small perturbations and for sensor operation at $\omega_{0,\text{REF}}$ (the resonance frequency of the SIR loaded with the REF material, which should be identical to the angular frequency providing a 90° electrical length to the sensing line covered by the same material).

The equivalence between both sensors will be demonstrated in the next section, devoted to sensor validation through simulation and experiment. Nevertheless, despite the similar behavior, the SIR resonator is significantly smaller than the equivalent 90° open-ended line. This has direct impact in the size of the sensing region, and, consequently, in the main figure of merit (FoM) of planar phase-variation sensors, as defined in the introduction section.

IV. SENSOR VALIDATION

For sensor validation, two SIR-terminated CPW based sensors have been designed and fabricated. The considered substrate is the *Rogers RO3010* with dielectric constant $\varepsilon_r = 10.2$, thickness $h = 1.27$ mm, and loss tangent $\tan\delta = 0.0022$. In the so-called sensor A, the SIR-terminated CPW is directly connected to the 50-Ω access line, whereas for sensor B, a pair ($N = 2$) of high/low impedance quarter wavelength transmission line sections is added between the SIR termination and the access line. The dimensions of the SIR terminated CPW are those indicated in the caption of Fig. 2. The impedances of the quarter-wavelength line sections are $Z_1 = 91\ \Omega$ and $Z_2 = 34.4\ \Omega$, resulting in the dimensions provided in the caption of Fig. 5, where the fabricated sensors are depicted. Sensor fabrication has been carried out by means of the *LPKF H100* milling machine. Contrary to similar sensors based on other resonant elements, in particular those reported in [51], where OCSRRs are used for sensing, sensors A and B do not require vias since the SIR resonators exhibit axial symmetry (contrary to the OCSRRs). Due to such axial symmetry, the appearance of the parasitic slot mode of the CPW is prevented, and vias and backside strips (with a functionality equivalent to the one of air-bridges, i.e., the electrical connection of the ground plane regions) are avoided.

We have also fabricated the fully distributed counterparts of sensors A and B, designated as A′ and B′, where the SIR resonators are replaced with 90° open-ended lines with impedance $Z_s = 70\ \Omega$, equivalent to the one of the SIRs (and given by equation 18). The photographs of the fabricated sensors A′ and B′ are also depicted in Fig. 5 (the dimensions of the quarter-wavelength open-ended sensing line are given in the caption).

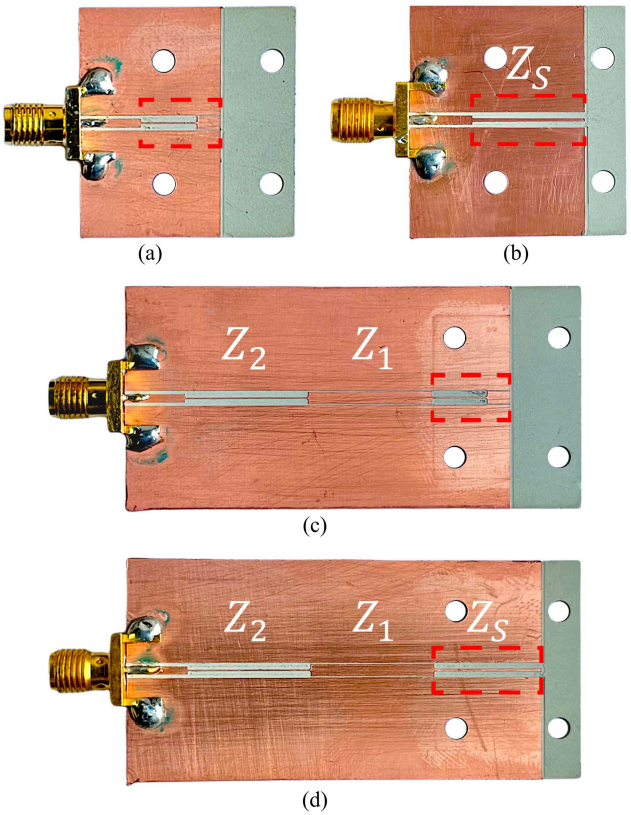

FIGURE 5. Typical Photographs of the fabricated sensors A (a), A′ (b), B (c), and B′ (d). The dimensions of the SIR-terminated CPW are given in Fig. 2. The dimensions of the high/low impedance CPW line sections (in mm) are: $w_1 = 1.6$, $G_1 = 0.2$, $l_1 = 16.67$, $w_2 = 0.2$, $G_2 = 0.9$, $l_2 = 16.5$. The dimensions of the high-impedance 90° open-ended sensing line (in mm) are: $w_S = 0.38$, $G_S = 0.81$, $l_S = 14.57$. In all the cases, the dimensions of the 50-Ω access lines (in mm) are: $w_0 = 1.1$, $G_0 = 0.45$, $l_0 = 8$.

Before experimental validation, the phase variation of the different sensors with the dielectric constant of the MUT, as well as the sensitivity, have been inferred by means of full-wave simulation using the *ANSYS HFSS* commercial software. For that purpose, the sensing regions are considered to be covered by semi-infinite MUTs with varying dielectric constant. The simulated phases obtained at the operating frequency, $f_{0,\mathrm{REF}} = \omega_{0,\mathrm{REF}}/2\pi = 2$ GHz, are depicted in Fig. 6. Such frequency is the resonance frequency of the SIR loaded with the REF material, identical to the frequency that provides an electrical length of 90° to the sensing lines of sensors A′ and B′. It should be mentioned that, actually, Fig. 6 depicts the differential phase, defined as the phase of the reflection coefficient for a given value of $\varepsilon_{\mathrm{MUT}}$ in reference to the one that results when the sensing region is covered by the REF material. The sensitivity has been inferred from the numerical derivative of the phase data (the results are also included in Fig. 6).

In view of Fig. 6, it can be seen that the sensitivities in the limit of small perturbations (i.e., for $\Delta C = 0$ pF, or $\varepsilon_{\mathrm{MUT}} = \varepsilon_{\mathrm{REF}}$) are very similar for the SIR-based and the open-ended 90° line-based sensors. The values, indicated in Fig. 6, agree with the theoretical predictions, given by expressions (19) or (23), to a very good approximation. These simulation results validate the sensitivity analysis of the previous section, as well as the equivalence between the SIR-based sensors and the fully distributed counterparts.

Thanks to the multiplicative effect generated by the normalized impedances of the high/low impedance 90° line sections (see expressions 23), the sensitivity for small perturbations is as high as −66.5° and −64.9° for sensors B and B′, respectively (simulated values). The FoM, or ratio between the sensitivity and the area of the sensing region expressed in terms of the squared guided wavelength, is found to be $\mathrm{FoM} = 3643°/\lambda^2$ and $\mathrm{FoM} = 2526°/\lambda^2$ for sensors B and B′, respectively. Note that for the calculation of the FoM, we have considered the area of the sensing region as the one given by the length of the sensing element (either the SIR, sensor B, or the quarter-wavelength sensing line, sensor B′), and a width that extends 2 mm beyond the ground planes (i.e., 6 mm). With a distance between ground planes of 2 mm in all the cases, it is considered that the electric field lines do not extend beyond that limit. This means that the improvement in the FoM is mainly due to the reduction in the length of the SIR, as compared to the quarter-wavelength resonator. These results clearly prove that by replacing the 90° open-ended sensing line of the distributed sensor with a SIR, the FoM can be substantially improved.

It should be mentioned that, in order to further increase the FoM (by decreasing the length of the sensor), we have surrounded the open end of the SIR-based sensor with a ground plane in order to obtain the same value of the SIR capacitance while reducing the length of the wide line section of the SIR. Particularly, we have considered a gap of 0.2 mm at the open end of the line. The effects of this modification have been analyzed through electromagnetic simulations, but it has been concluded that it is not possible to obtain a competitive advantage by this procedure, since the reduction of the sensing area is approximately 1%.

Experimental validation has been carried out by covering the sensing regions of the four designed and fabricated sensors with several commercially available (uncladded) microwave substrates, with a MUT sample (PLA) fabricated with a 3D printer (the *Ultimaker 3 Extended*), and by leaving the sensing region unloaded (i.e., surrounded by air). The thickness of the MUT samples is roughly 3 mm. With such thickness, the samples can be considered to be semi-infinite in the vertical direction (stacking of two 1.5-mm thick samples, available in our laboratory, has been carried out for that purpose). The specific samples exhibit dielectric constants of 2.2 (estimated for PLA), 3.55 (for *Rogers RO4003C*), 4.4 (for *FR4*), and 10.2 (for *Rogers RO3010*). The measured differential phases at the operating frequency for such MUTs and air, inferred by means of the *Keysight 85072A* vector network analyzer, are also included in Fig. 6. The measurements have been performed three times, in order to ensure repetitiveness (the corresponding error bars are included in Fig. 6). The agreement between the measured data points and the simulated values is very good in all the cases. This means that the curves corresponding to the simulated values

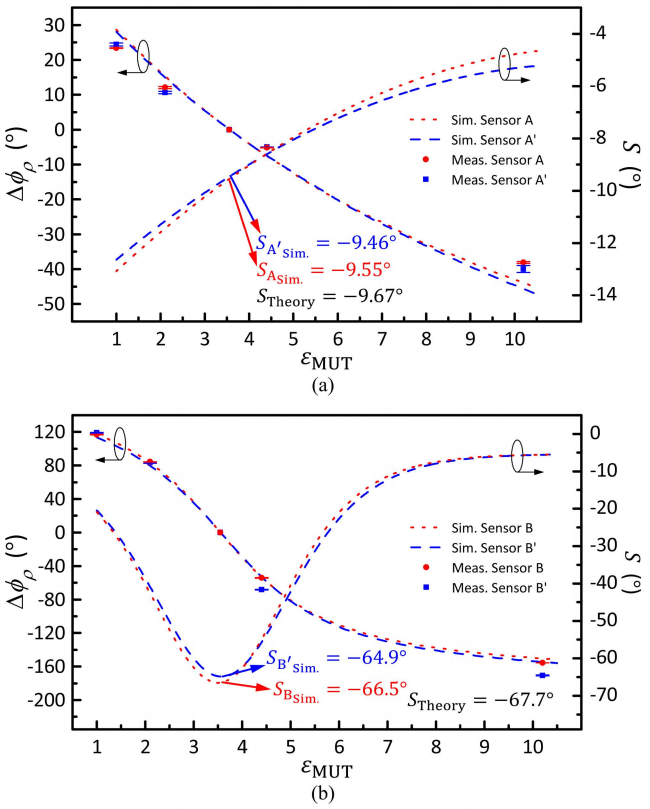

FIGURE 6. Typical phase ($\Delta\phi_\rho = \phi_\rho - \phi_{\rho,\varepsilon REF}$) at $f_{0,REF}$ and sensitivity for the designed and fabricated sensors. (a) Sensors A and A'; (b) sensors B and B'.

can be used to infer the dielectric constant of any hypothetical material from the measurement of the differential phase.

As expected, sensitivity enhancement degrades the sensor linearity, as revealed by the curves of Fig. 6. This means that for dielectric measurements with a relatively large input dynamic range, it may be convenient to design the sensor with moderate value of the sensitivity, at the expense of a limited resolution. By contrast, for the use of the sensor as comparator, e.g., to determine potential defects, irregularities, or changes between a certain sample and a well-known reference (REF) sample, the sensitivity should be high in order to resolve (and hence detect) tiny variations in the sample under test (or MUT). Such variations are typically manifested through changes in the dielectric constant, and are therefore detectable with the proposed sensor, as far as the sensitivity in the vicinity of the REF sample is sufficiently high.

To illustrate the potential of the proposed sensors to detect small defects in samples, we have deliberately drilled arrays of holes of different densities in the REF sample (equivalent to reduce the dielectric constant). Photographs of the different defected samples and the measured differential phases, using sensors A and B, at the operating frequency are shown in Fig. 7. The measurements have been performed 3 times in order to analyze the repetitiveness, as well as the effects of potential inaccuracies related to sample positioning (the corresponding error bars are included in Fig. 7). The enhanced capacity to detect the defects by using sensor B can be clearly

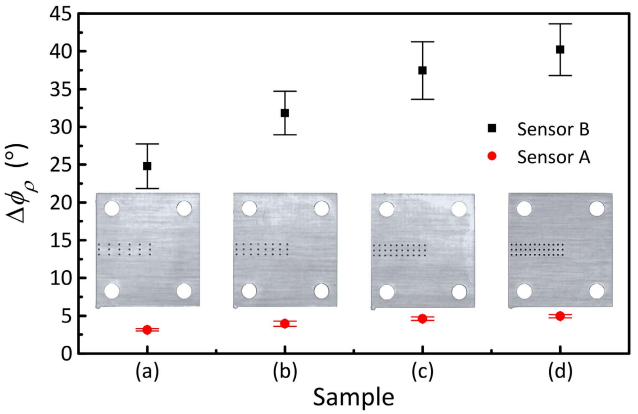

FIGURE 7. Measured differential phases for the different samples using sensors A and B. The set of defected samples, inferred from the REF samples by drilling arrays of holes of different densities, is shown with the corresponding phase measurements.

appreciated. This is due to the higher sensitivity of sensor B at $\varepsilon_{MUT} = \varepsilon_{REF}$. With the results of Fig. 7, it is clear that the proposed sensor B is useful to detect small variations in the dielectric constant in the vicinity of that of the REF sample.

It should be mentioned that in the analysis of the previous section, as well as in the validation of the designed and fabricated sensors of the present section, it has been assumed that the thickness of the MUT fulfills the semi-infinite MUT approximation. Compact expressions providing the sensitivity for small perturbations have been obtained and validated (19 or 23) by virtue of such approximation. Nevertheless, the sensors are also useful for determining the dielectric constant of thinner samples, not subjected to the semi-infinite approximation. For that purpose, curves equivalent to those of Fig. 6 for thinner MUT samples (with predefined thickness) can be generated. Thus, the considered approximation does not represent a loss of generality of the proposed sensors. However, for thin MUT characterization, it is important to know the thickness of the sample in order to use the corresponding calibration curve.

V. DISCUSSION

An important aspect of the proposed SIR-based sensors concerns the lack of cross-sensitivity of the output variable, the phase of the reflection coefficient, with the loss factor of the MUT (or loss tangent, $\tan\delta_{MUT}$). This has been corroborated from electromagnetic simulation using *ANSYS HFSS*. Thus, Fig. 8(a) depicts the phase of the reflection coefficient at the operating frequency for the sensor based only on the SIR and access line (sensor A), as a function of both the dielectric constant and loss tangent of the MUT. It can be clearly appreciated that the phase of the reflection coefficient depends only on the dielectric constant of the MUT, being independent of the loss tangent. The fact that the device does not exhibit cross-sensitivity with the loss tangent of the MUT is relevant, since this means that the dielectric constant of the MUT, the input variable, can be retrieved regardless of the loss factor of the MUT.

Let us suppose that a second output variable is considered for the (possible) determination of the loss tangent of the MUT. Obviously, the magnitude of the reflection coefficient at resonance should be influenced by the overall losses of the device, including $\tan\delta_{\mathrm{MUT}}$. Therefore, it follows that such magnitude is the canonical second output variable, potentially useful for retrieving $\tan\delta_{\mathrm{MUT}}$. Fig. 8(b) depicts the dependence of the magnitude of the reflection coefficient at resonance with both $\tan\delta_{\mathrm{MUT}}$ and $\varepsilon_{\mathrm{MUT}}$. Contrary to the phase, the magnitude of the reflection coefficient at resonance depends on both the loss factor and the dielectric constant of the MUT. In other words, this second output variable exhibits cross sensitivity with the dielectric constant of the MUT. Thus, the determination of the loss tangent of the MUT with these sensors is not simple, since the surface of Fig. 8(b) cannot be considered as a calibration surface. The main reason is that, in experiment, there are several sources of losses, difficult to account in simulation, and generating such calibration surface from experiment is not possible due to the lack of a set of representative data points. On the other hand, a semi-analytical method for retrieving the loss tangent of the MUT, similar to that reported in [51] in reference to OCSRR-based reflective-mode phase-variation sensors, and based on the circuit model of the SIR-based sensor by including losses, is not possible, at least for MUTs with moderate and low loss levels. The reason is that the losses of the access lines and substrate obscure the losses associated to the MUT, as it has been demonstrated from electromagnetic simulations, not shown.

Thus, with the SIR-based CPW sensors reported in this work, the dielectric constant of the MUT can be accurately predicted, but not the loss tangent. Nevertheless, there are many variables related to the dielectric constant of the MUT that can potentially be measured with these sensors, e.g., liquid composition in mixtures, or physical variables, such as temperature or humidity, among others (in this case, functional materials with a dielectric constant dependent on the physical variable to be sensed might be necessary). Moreover, by virtue of the highly achievable sensitivity, these sensors can be used for the detection of tiny defects in samples, as it has been demonstrated in the previous section.

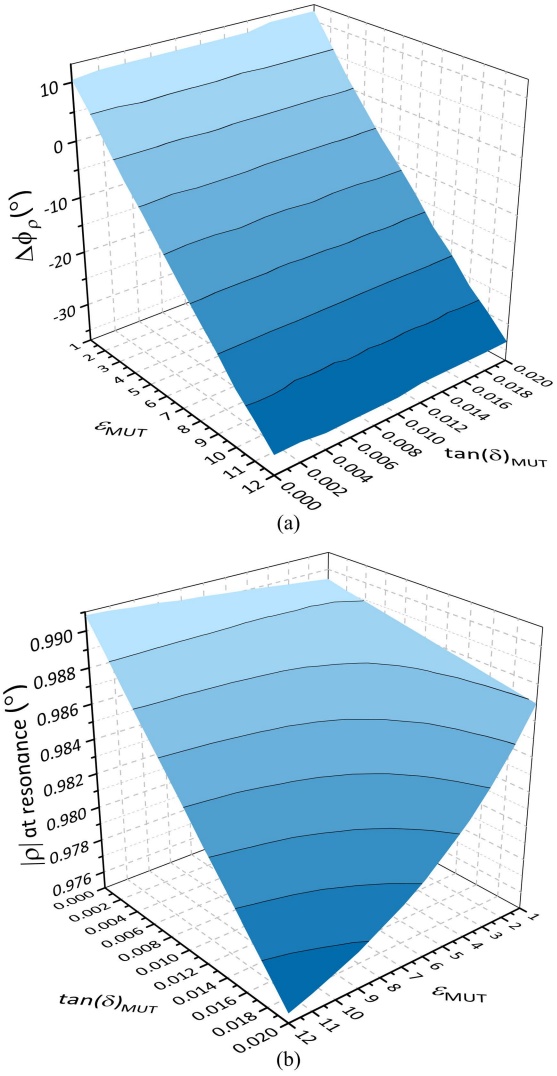

FIGURE 8. Phase of the reflection coefficient at the operating frequency (a), and magnitude of the reflection coefficient at resonance (b) for the SIR-based sensor A, inferred from electromagnetic simulation.

VI. COMPARISON WITH OTHER PHASE VARIATION SENSORS

Table 1 includes a list of various phase-variation sensors recently reported, and their main relevant parameters, as well as other characteristics of interest. The table is restricted to phase-variation sensors, since comparing sensors with different sensing principle is difficult (and even meaningless). In view of the table, the proposed sensor B exhibits a good FoM, by virtue of the small area of the sensing region. Note that the FoM is superior to the one of the equivalent sensor implemented by means of a 90° open-ended sensing line (sensor B′). As explained, the reason is the shorter length of the sensing region in the SIR-based sensor B, as compared to the distributed sensor counterpart B′ (by contrast, the width is identical, i.e., 6 mm, in both sensors). The sensitivity in the reflective-mode sensor reported in [48] is huge, and for this main reason, the FoM in that sensor is so high, despite the fact that the size of the sensing region is not as small as the one of the SIR-based sensors presented in this paper.

Nevertheless, further increasing the sensitivity in the proposed sensors, as well as in other reflective-mode phase variation sensors based on high/low impedance quarter-wavelength line sections, is possible by merely cascading additional high/low impedance line sections to the sensing structure. It should be mentioned that sensors B and B′ in this paper, as well as the optimum sensor presented in [48], include two ($N = 2$) high/low impedance 90° line sections (plus the sensing line, or SIR in the present paper). However, the sensors presented in this paper are implemented in CPW technology, whereas the sensors in [48] were fabricated in microstrip technology in a different substrate (with the possibility of implementing 90° line sections with a

TABLE 1. Comparison of various phase variation-sensors.

Ref.	*Mode / Sensing element**	f_0 (GHz)	*Size*** (λ^2)	*Max. Sensitivity*	*FoM* ($^o/\lambda^2$)
[48]	REFLECT. / TL	2.0	0.025	528.7º	21148
[49]	REFLECT. / TL	2.0	0.100	45.5º	455
[27]	TRANS. / CRLH	2.3	---	600 dB	---
[29]	TRANS. / TL	---	---	54.8º	---
[33]	TRANS. / TL	6.0	12.90	415.6º	32.2
[35]	TRANS. / EIW	---	0.075	25.3 dB	---
[36]	TRANS. / TL	2.0	0.020	17.6 dB	---
[52]	TRANS. / SW	3.0	0.030	7.7º	257
[53]	TRANS. / SW	2.0	0.040	20.0º	500
[51]	REFLECT. / OCSRR	2.0	0.015	83.35º	5643
Sens. B'	REFLECT. / TL	2.0	0.026	64.9º	2526
Sens. B	**REFLECT. / SIR**	**2.0**	**0.018**	**66.5º**	**3643**

* REFLECT. and TRANS. stands for reflective- and transmission-mode, respectively. The sensing elements are ordinary transmission lines (TL), composite right/left handed lines (CRLH), electroinductive-wave transmission lines (EIW), slow-wave transmission lines (SW), open complementary split ring resonators (OCSRR), or step impedance resonators (SIR).
**The size corresponds to the sensing region, not to the whole sensing structure.

larger impedance contrast). Indeed, the main objective of this paper has not been to design and fabricate a reflective-mode phase-variation sensor with the highest reported sensitivity (this would be possible by simply adding further high/low impedance line sections as indicated), but to demonstrate that there is an equivalence between the reported SIR-based sensors and the distributed reflective-mode phase-variation sensors based on open-ended quarter-wavelength sensing lines, and that the FoM is better in the sensors implemented by the SIR sensing resonators, by virtue of their small electrical size.

Table 1 includes transmission-mode sensors based on line meandering [33], a technique to boost up the sensitivity by considering long sensing lines with mode shape factors. However, the resulting FoM is very limited as compared to those of the sensors reported in [48], [49], [51], and sensors B and B′ of the present work. An alternative strategy to enhance the sensitivity in phase-variation sensors is to replace the ordinary sensing lines with artificial lines. For example, in [52], [53], the reported sensors are implemented by means of slow-wave transmission lines. The FoM in such sensors is reasonably good, at least it is better than the one of the meander-line based sensor of [33], but not as good as those of the sensors of [48], [49], [51], and sensors B and B′ of this work. Finally, let us mention that in the phase-variation sensors reported in [27], [35], [36], the phase is converted to magnitude, and for this reason, the FoM in such sensors is not reported (nevertheless, the sensitivity of the sensors of [27] is very good).

The achieved FoM in sensor B is of the same order of magnitude as the one of the reflective-mode phase-variation sensor based on an open-complementary split ring resonator (OCSRR) reported in [51]. Thus, such sensors, both based on semi-lumped sensing resonators are comparable. However, the SIR resonator is simply described by a series LC resonator, contrary to the OCSRR, that needs the inclusion of parasitic elements, besides a parallel LC resonant tank, for an accurate modeling. Moreover, since the OCSRR does not exhibit any symmetry plane, vias are required in order to avoid the generation of the parasitic slot mode. Thus, in summary, the SIR-based sensors of the present paper exhibit more simple design and fabrication, and are considered to be the preferred option for the implementation of reflective-mode phase-variation sensors in CPW technology. The equivalence with the distributed quarter-wavelength-based sensor, but the smaller size of the SIR sensor, and comparable design and fabrication burden, justify the previous statement. Note also that it is possible to further improve the figure of merit of sensor B by merely cascading additional high/low impedance quarter-wavelength transmission line sections.

VII. CONCLUSION

In conclusion, highly-sensitive one-port reflective-mode phase-variation sensors useful for the measurement of the dielectric constant of solid samples have been presented in this paper. The sensing element in such sensors is an electrically small planar semi-lumped resonator, the step-impedance resonator (SIR), which is connected as a termination load of a cascade of high/low impedance quarter-wavelength transmission line sections. With the use of such step-impedance transmission line configuration, the sensitivity can be substantially enhanced, by keeping unaltered the size of the sensing region, determined by the size of the SIR resonator. The (maximum) sensitivity achieved in one of the proposed sensors (designated as sensor B), based on the sensing SIR plus two additional quarter-wavelength line sections with alternating low and high impedance, is as high as $-66.5°$, the output variable being the phase of the reflection coefficient, and the input variable the dielectric constant of the MUT sample. The achieved figure of merit (FoM) in such sensor, defined as the ratio of the maximum sensitivity and the area of the sensing region expressed in terms of the guided wavelength, is FoM $= 3642°/\lambda^2$, a competitive value that can be further increased by merely adding further quarter-wavelength high/low transmission line sections. It has also been demonstrated in this paper that the effects of both MUT and sensor losses do not affect the dependence of the phase of the reflection coefficient (the output variable) with the dielectric constant of the MUT, provided losses are small. In other words, the phase of the reflection coefficient does not exhibit cross sensitivity with the loss factor of the MUT. Finally, it has been demonstrated in the paper that the proposed SIR-based sensors are equivalent to their distributed counterparts, based on the replacement of the SIR resonator with an open-ended quarter-wavelength transmission line resonator. Indeed, an expression that provides the characteristic impedance of the quarter-wavelength sensing line (from the inductance and capacitance of the SIR resonator), that is necessary to obtain the same sensitivity has been inferred. However, the SIR-based sensors exhibit a superior FoM by virtue of their smaller electrical size, as compared to the quarter-wavelength sensing lines. In this paper, sensor validation has been carried out by considering solid

samples. However, this type of sensors is also useful for the characterization of liquids (dielectric characterization, composition, determination of solute content in diluted solutions, etc.). For sensitivity optimization, the operating frequency in this case should be tuned to the resonance frequency of the SIR loaded with the reference liquid. Nevertheless, for significant variations in the permittivity of the liquids under study, it might be convenient to limit the sensitivity in favor of the sensor linearity. For liquid characterization, either fluidic channels or liquid containers should be added on top of the sensing area. Alternatively, submersible sensors can be envisaged, a reasonable approach for liquid measurements. The reason is that this one-port reflective-mode phase-variation sensors can be considered to be sensing probes, where, for measurement, it suffices to introduce the sensing element (either the SIR or the quarter-wavelength sensing line) within the liquid. Nevertheless, protection of the high/low impedance quarter-wavelength line sections is required. Work is in progress in this direction, but this is the subject of a future work.

APPENDIX
EQUIVALENCE BETWEEN A 90° OPEN-ENDED SENSING LINE AND A SERIES LC SENSING RESONATOR

Let us consider an open-ended terminated line with impedance Z_s and phase $\phi_s = \pi/2$ when it is loaded with an MUT, which is considered to be the REF material, at the frequency designated as $\omega_{0,\mathrm{REF}}$. Under these loading conditions and frequency, the input reactance is null, due to the impedance inversion of the quarter-wavelength open-ended line. However, if the dielectric constant of the MUT is slightly perturbed, and losses are neglected, the input reactance changes to [63]

$$\chi_{\mathrm{in,line}} = Z_s \Delta\phi_s \tag{A.1}$$

where $\Delta\phi_s$ is the variation experienced by the phase of the line due to the changes in the dielectric constant of the MUT.

Let us now consider a series LC resonator describing a planar resonant particle such as a SIR-terminated CPW, and let us assume that the particle resonates at the angular frequency $\omega_{0,\mathrm{REF}}$, when it is loaded with the REF material (providing a capacitance C'_{REF} to the SIR). The reactance at such frequency is obviously null, unless the MUT exhibits different dielectric constant than the REF material. This potential variation in the dielectric constant of the MUT perturbs the capacitance of the SIR a quantity ΔC, and the reactance, in the limit of small perturbations, at $\omega_{0,\mathrm{REF}}$ can be expressed as

$$\chi_{\mathrm{in}} = \omega_{0,\mathrm{REF}} L \frac{\Delta C}{C'_{\mathrm{REF}}} \tag{A.2}$$

On the other hand, $\Delta\phi_{\mathrm{s}}$ can be expressed as

$$\Delta\phi_s = \omega_{0,\mathrm{REF}} \left(\sqrt{L_l (C_l + \Delta C_l)} - \sqrt{L_l C_l} \right) \tag{A.3}$$

where L_l and C_l are the inductance and capacitance, respectively, of the line covered with the REF material (of electrical length $\pi/2$), and ΔC_l is the variation of the line capacitance caused by the MUT. For small perturbations, ΔC_l is small as compared to C_l, and (A.3) can be approximated by

$$\begin{aligned} \Delta\phi_s &= \omega_{0,\mathrm{REF}} \sqrt{L_l C_l} \left(\sqrt{1 + \frac{\Delta C_l}{C_l}} - 1 \right) \\ &\approx \omega_{0,\mathrm{REF}} \sqrt{L_l C_l} \left(\frac{\Delta C_l}{2C_l} \right) \end{aligned} \tag{A.4}$$

or

$$\Delta\phi_s = \frac{\pi}{2} \cdot \frac{\Delta C_l}{2C_l} \tag{A.5}$$

Forcing (A.1) and (A.2) to be identical, using (A.5), and identifying $\Delta C_l/C_l$ with $\Delta C/C'_{\mathrm{REF}}$, the following equivalence is obtained

$$Z_s = \frac{4L\omega_{0,\mathrm{REF}}}{\pi} = \frac{4}{\pi}\sqrt{\frac{L}{C'_{\mathrm{REF}}}} \tag{A.6}$$

Therefore, for small perturbations, the response of the sensor based on the SIR-terminated CPW and the one of the sensor based on a quarter-wavelength open-ended sensing line are expected to be identical provided the inductance and capacitance of the SIR loaded with the REF material are selected according to

$$L = \frac{\pi Z_s}{4\omega_{0,\mathrm{REF}}}, \quad C'_{\mathrm{REF}} = \frac{4}{\pi Z_s \omega_{0,\mathrm{REF}}} \tag{A.7}$$

and the equivalence between ΔC and $\Delta\phi_s$ is given by:

$$\Delta\phi_s = \pi \frac{\Delta C}{4C'_{\mathrm{REF}}} \tag{A.8}$$

Note that the relative variation of the line capacitance of a CPW, $\Delta C_l/C_l$, as consequence of a change in the dielectric constant of the MUT, is identical to the relative variation experienced by the capacitance of the SIR, $\Delta C/C'_{\mathrm{REF}}$. Consequently, if the equivalence given by (A.6), or by (A.7), is satisfied, identical sensitivities in the limit of small perturbations are expected for both sensors, as it has been demonstrated in Section IV.

REFERENCES

[1] P. Wei, B. Morey, T. Dyson, N. McMahon, Y. Y. Hsu, S. Gazman, L. Klinker, B. Ives, K. Dowling, and C. Rafferty, "A conformal sensor for wireless sweat level monitoring," in *Proc. Sensors*, Nov. 2013, pp. 1–4.

[2] L. Su, X. Huang, W. Guo, and H. Wu, "A flexible microwave sensor based on complementary spiral resonator for material dielectric characterization," *IEEE Sensors J.*, vol. 20, no. 4, pp. 1893–1903, Feb. 2020.

[3] M. M. Rodgers, V. M. Pai, and R. S. Conroy, "Recent advances in wearable sensors for health monitoring," *IEEE Sensors J.*, vol. 15, no. 6, pp. 3119–3126, Jun. 2014.

[4] K. Grenier, D. Dubuc, P. E. Poleni, M. Kumemura, H. Toshiyoshi, T. Fujii, and H. Fujita, "Integrated broadband microwave and microfluidic sensor dedicated to bioengineering," *IEEE Trans. Microw. Theory Techn.*, vol. 57, no. 12, pp. 3246–3253, Dec. 2009.

[5] T. Chretiennot, D. Dubuc, and K. Grenier, "A microwave and microfluidic planar resonator for efficient and accurate complex permittivity characterization of aqueous solutions," *IEEE Trans. Microw. Theory Techn.*, vol. 61, no. 2, pp. 972–978, Feb. 2012.

[6] A. Ebrahimi, W. Withayachumnankul, S. Al-Sarawi, and D. Abbott, "High-sensitivity metamaterial-inspired sensor for microfluidic dielectric characterization," *IEEE Sensors J.*, vol. 14, no. 5, pp. 1345–1351, May 2014.

[7] P. Vélez, L. Su, K. Grenier, J. Mata-Contreras, D. Dubuc, and F. Martín, "Microwave microfluidic sensor based on a microstrip splitter/combiner configuration and split ring resonators (SRR) for dielectric characterization of liquids," *IEEE Sensors J.*, vol. 17, no. 20, pp. 6589–6598, Oct. 2017.
[8] P. Vélez, K. Grenier, J. Mata-Contreras, D. Dubuc, and F. Martín, "Highly-sensitive microwave sensors based on open complementary split ring resonators (OCSRRs) for dielectric characterization and solute concentration measurement in liquids," *IEEE Access*, vol. 6, pp. 48324–48338, 2018.
[9] P. Vélez, J. Muñoz-Enano, K. Grenier, J. Mata-Contreras, D. Dubuc, and F. Martín, "Split ring resonator (SRR) based microwave fluidic sensor for electrolyte concentration measurements," *IEEE Sensors J.*, vol. 19, no. 7, pp. 2562–2569, Apr. 2019.
[10] A. Salim, S.-H. Kim, J. Y. Park, and S. Lim, "Microfluidic biosensor based on microwave substrate-integrated waveguide cavity resonator," *J. Sensors*, vol. 2018, pp. 1–13, Feb. 2018.
[11] M. H. Zarifi, H. Sadabadi, S. H. Hejazi, M. Daneshmand, and A. Sanati-Nezhad, "Noncontact and nonintrusive microwave-microfluidic flow sensor for energy and biomedical engineering," *Sci. Rep.*, vol. 8, no. 1, pp. 1–10, Dec. 2018.
[12] J. Castillo-León and W. E. Svendsen, *Lab-on-a-Chip Devices and Micro-Total Analysis Systems: A Practical Guide*. New York, NY, USA: Springer, Nov. 2014.
[13] M. Puentes, C. Weiss, M. Schussler, and R. Jakoby, "Sensor array based on split ring resonators for analysis of organic tissues," in *IEEE MTT-S Int. Microw. Symp. Dig.*, Baltimore, MD, USA, Jun. 2011, pp. 1–4.
[14] M. Schueler, C. Mandel, M. Puentes, and R. Jakoby, "Metamaterial inspired microwave sensors," *IEEE Microw. Mag.*, vol. 13, no. 2, pp. 57–68, Mar. 2012.
[15] M. S. Boybay and O. M. Ramahi, "Material characterization using complementary split-ring resonators," *IEEE Trans. Instrum. Meas.*, vol. 61, no. 11, pp. 3039–3046, Nov. 2012.
[16] C.-S. Lee and C.-L. Yang, "Complementary split-ring resonators for measuring dielectric constants and loss tangents," *IEEE Microw. Wireless Compon. Lett.*, vol. 24, no. 8, pp. 563–565, Aug. 2014.
[17] C.-L. Yang, C.-S. Lee, K.-W. Chen, and K.-Z. Chen, "Noncontact measurement of complex permittivity and thickness by using planar resonators," *IEEE Trans. Microw. Theory Techn.*, vol. 64, no. 1, pp. 247–257, Jan. 2016.
[18] L. Su, J. Mata-Contreras, P. Vèlez, and F. Martín, "Estimation of the complex permittivity of liquids by means of complementary split ring resonator (CSRR) loaded transmission lines," in *IEEE MTT-S Int. Microw. Symp. Dig.*, Pavia, Italy, Sep. 2017, pp. 20–22.
[19] L. Su, J. Mata-Contreras, P. Vélez, A. Fernández-Prieto, and F. Martín, "Analytical method to estimate the complex permittivity of oil samples," *Sensors*, vol. 18, p. 984, Mar. 2018.
[20] A. K. Jha, N. Delmonte, A. Lamecki, M. Mrozowski, and M. Bozzi, "Design of microwave-based angular displacement sensor," *IEEE Microw. Wireless Compon. Lett.*, vol. 29, no. 4, pp. 306–308, Apr. 2019.
[21] A. K. Horestani, J. Naqui, Z. Shaterian, D. Abbott, C. Fumeaux, and F. Martín, "Two-dimensional alignment and displacement sensor based on movable broadside-coupled split ring resonators," *Sens. Actuators A, Phys.*, vol. 210, pp. 18–24, Apr. 2014.
[22] J. Naqui, C. Damm, A. Wiens, R. Jakoby, L. Su, and F. Martin, "Transmission lines loaded with pairs of magnetically coupled stepped impedance resonators (SIRs): Modeling and application to microwave sensors," in *IEEE MTT-S Int. Microw. Symp. Dig.*, Tampa, FL, USA, Jun. 2014, pp. 1–4.
[23] L. Su, J. Naqui, J. Mata-Contreras, and F. Martín, "Modeling metamaterial transmission lines loaded with pairs of coupled split ring resonators," *IEEE Antennas Wireless Propag. Lett.*, vol. 14, pp. 68–71, 2015.
[24] L. Su, J. Naqui, J. Mata-Contreras, and F. Martín, "Modeling and applications of metamaterial transmission lines loaded with pairs of coupled complementary split ring resonators (CSRRs)," *IEEE Antennas Wireless Propag. Lett.*, vol. 15, pp. 154–157, 2016.
[25] J. Naqui, C. Damm, A. Wiens, R. Jakoby, L. Su, J. Mata-Contreras, and F. Martín, "Transmission lines loaded with pairs of stepped impedance resonators: Modeling and application to differential permittivity measurements," *IEEE Trans. Microw. Theory Techn.*, vol. 64, no. 11, pp. 3864–3877, Nov. 2016.
[26] L. Su, J. Mata-Contreras, P. Vélez, and F. Martín, "Splitter/combiner microstrip sections loaded with pairs of complementary split ring resonators (CSRRs): Modeling and optimization for differential sensing applications," *IEEE Trans. Microw. Theory Techn.*, vol. 64, no. 12, pp. 4362–4370, Dec. 2016.
[27] C. Damm, M. Schüßler, M. Puentes, H. Maune, M. Maasch, and R. Jakoby, "Artificial transmission lines for high sensitive microwave sensors," in *Proc. IEEE Sensors Conf.*, Christchurch, New Zealand, Oct. 2009, pp. 755–758.
[28] P. Vélez, L. Su, J. Mata-Contreras, F. Martín, K. Grenier, and D. Dubuc, "Modeling and analysis of pairs of open complementary split ring resonators (OCSRRs) for differential permittivity sensing," in *MTT-S*, Pavia, Italy, Sep. 2017, pp. 20–22.
[29] F. J. Ferrández-Pastor, J. M. García-Chamizo, and M. Nieto-Hidalgo, "Electromagnetic differential measuring method: Application in microstrip sensors developing," *Sensors*, vol. 17, no. 7, p. 1650, 2017.
[30] A. Ebrahimi, J. Scott, and K. Ghorbani, "Transmission lines terminated with LC resonators for differential permittivity sensing," *IEEE Microw. Wireless Compon. Lett.*, vol. 28, no. 12, pp. 1149–1151, Dec. 2018.
[31] B. Ebrahimi, J. Scott, and K. Ghorbani, "Differential sensors using microstrip lines loaded with two split ring resonators," *IEEE Sensors J.*, vol. 18, no. 14, pp. 5786–5793, Jul. 2018.
[32] P. Vélez, J. Muñoz-Enano, M. Gil, J. Mata-Contreras, and F. Martín, "Differential microfluidic sensors based on dumbbell-shaped defect ground structures in microstrip technology: Analysis, optimization, and applications," *Sensors*, vol. 19, p. 3189, Jul. 2019.
[33] J. Muñoz-Enano, P. Vélez, M. Gil, and F. Martín, "An analytical method to implement high sensitivity transmission line differential sensors for dielectric constant measurements," *IEEE Sensors J.*, vol. 20, no. 1, pp. 178–184, Jan. 2020.
[34] P. Vélez, J. Muñoz-Enano, and F. Martín, "Differential sensing based on quasi-microstrip-mode to slot-mode conversion," *IEEE Microw. Wireless Compon. Lett.*, vol. 29, pp. 690–692, 2019.
[35] M. Gil, P. Vélez, F. Aznar, J. Muñoz-Enano, and F. Martín, "Differential sensor based on electro-inductive wave (EIW) transmission lines for dielectric constant measurements and defect detection," *IEEE Trans. Antennas Propag.*, vol. 68, pp. 1876–1886, 2020.
[36] J. Muñoz-Enano, P. Vélez, M. Gil, J. Mata-Contreras, and F. Martín, "Differential-mode to common-mode conversion detector based on rat-race couplers: Analysis and application to microwave sensors and comparators," *IEEE Trans. Microw. Theory Techn.*, vol. 68, no. 4, pp. 1312–1325, Apr. 2020.
[37] J. Naqui, M. Durán-Sindreu, and F. Martín, "Novel sensors based on the symmetry properties of split ring resonators (SRRs)," *Sensors*, vol. 11, no. 8, pp. 7545–7553, 2011.
[38] J. Naqui, M. Durán-Sindreu, and F. Martín, "Alignment and position sensors based on split ring resonators," *Sensors*, vol. 12, no. 9, pp. 11790–11797, Aug. 2012.
[39] A. K. Horestani, C. Fumeaux, S. F. Al-Sarawi, and D. Abbott, "Displacement sensor based on diamond-shaped tapered split ring resonator," *IEEE Sensors J.*, vol. 13, no. 4, pp. 1153–1160, Apr. 2013.
[40] A. K. Horestani, D. Abbott, and C. Fumeaux, "Rotation sensor based on horn-shaped split ring resonator," *IEEE Sensors J.*, vol. 13, no. 8, pp. 3014–3015, Aug. 2013.
[41] J. Naqui and F. Martín, "Transmission lines loaded with bisymmetric resonators and their application to angular displacement and velocity sensors," *IEEE Trans. Microw. Theory Techn.*, vol. 61, no. 12, pp. 4700–4713, Dec. 2013.
[42] J. Naqui and F. Martín, "Angular displacement and velocity sensors based on electric-LC (ELC) loaded microstrip lines," *IEEE Sensors J.*, vol. 14, no. 4, pp. 939–940, Apr. 2014.
[43] A. K. Horestani, J. Naqui, D. Abbott, C. Fumeaux, and F. Martín, "Two-dimensional displacement and alignment sensor based on reflection coefficients of open microstrip lines loaded with split ring resonators," *Electron. Lett.*, vol. 50, no. 8, pp. 620–622, Apr. 2014.
[44] A. Ebrahimi, W. Withayachumnankul, S. F. Al-Sarawi, and D. Abbott, "Metamaterial-inspired rotation sensor with wide dynamic range," *IEEE Sensors J.*, vol. 14, no. 8, pp. 2609–2614, Aug. 2014.
[45] J. Naqui, J. Coromina, B. Karami-Horestani, C. Fumeaux, and F. Martín, "Angular displacement and velocity sensors based on coplanar waveguides (CPWs) loaded with S-shaped split ring resonator (S-SRR)," *Sensors*, vol. 15, no. 5, pp. 9628–9650, 2015.
[46] J. Mata-Contreras, C. Herrojo, and F. Martín, "Application of split ring resonator (SRR) loaded transmission lines to the design of angular displacement and velocity sensors for space applications," *IEEE Trans. Microw. Theory Techn.*, vol. 65, no. 11, pp. 4450–4460, Nov. 2017.

[47] J. Mata-Contreras, C. Herrojo, and F. Martín, "Detecting the rotation direction in contactless angular velocity sensors implemented with rotors loaded with multiple chains of split ring resonators (SRRs)," *IEEE Sensors J.*, vol. 18, no. 17, pp. 7055–7065, Sep. 2018.

[48] J. Munoz-Enano, P. Velez, L. Su, M. Gil, P. Casacuberta, and F. Martin, "On the sensitivity of reflective-mode phase-variation sensors based on open-ended stepped-impedance transmission lines: Theoretical analysis and experimental validation," *IEEE Trans. Microw. Theory Techn.*, vol. 69, no. 1, pp. 308–324, Jan. 2021.

[49] L. Su, J. Munoz-Enano, P. Velez, P. C. Orta, M. Gil, and F. Martin, "Highly sensitive phase variation sensors based on step-impedance coplanar waveguide (CPW) transmission lines," *IEEE Sensors J.*, vol. 21, no. 3, pp. 2864–2872, Feb. 2021.

[50] P. Casacuberta, J. Muñoz-Enano, P. Vélez, L. Su, M. Gil, and F. Martín, "Highly sensitive reflective-mode defect detectors and dielectric constant sensors based on open-ended stepped-impedance transmission lines," *Sensors*, vol. 20, no. 21, p. 6236, Oct. 2020.

[51] L. Su, J. Muñoz-Enano, P. Vélez, M. Gil-Barba, P. Casacuberta, and F. Martín, "Highly sensitive reflective-mode phase-variation permittivity sensor based on a coplanar waveguide (CPW) terminated with an open complementary split ring resonator (OCSRR)," *IEEE Access*, vol. 9, pp. 27928–27944, 2021.

[52] J. Coromina, J. Munoz-Enano, P. Velez, A. Ebrahimi, J. Scott, K. Ghorbani, and F. Martin, "Capacitively-loaded slow-wave transmission lines for sensitivity improvement in phase-variation permittivity sensors," in *Proc. 50th Eur. Microw. Conf. (EuMC)*, Utrecht, The Netherlands, Jan. 2021, pp. 491–494.

[53] A. Ebrahimi, J. Coromina, J. Munoz-Enano, P. Velez, J. Scott, K. Ghorbani, and F. Martin, "Highly sensitive phase-variation dielectric constant sensor based on a capacitively-loaded slow-wave transmission line," *IEEE Trans. Circuits Syst. I, Reg. Papers*, vol. 68, no. 7, pp. 2787–2799, Jul. 2021.

[54] J. Munoz-Enano, P. Velez, L. Su, M. Gil-Barba, and F. Martin, "A reflective-mode phase-variation displacement sensor," *IEEE Access*, vol. 8, pp. 189565–189575, 2020.

[55] A. K. Jha, A. Lamecki, M. Mrozowski, and M. Bozzi, "A highly sensitive planar microwave sensor for detecting direction and angle of rotation," *IEEE Trans. Microw. Theory Techn.*, vol. 68, no. 4, pp. 1598–1609, Apr. 2020.

[56] A. K. Horestani, Z. Shaterian, and F. Martin, "Rotation sensor based on the cross-polarized excitation of split ring resonators (SRRs)," *IEEE Sensors J.*, vol. 20, no. 17, pp. 9706–9714, Sep. 2020.

[57] N. Kazemi, K. Schofield, and P. Musilek, "A high-resolution reflective microwave planar sensor for sensing of vanadium electrolyte," *Sensors*, vol. 21, no. 11, p. 3759, May 2021.

[58] A. Velez, F. Aznar, J. Bonache, M. C. Velazquez-Ahumada, J. Martel, and F. Martin, "Open complementary split ring resonators (OCSRRs) and their application to wideband CPW band pass filters," *IEEE Microw. Wireless Compon. Lett.*, vol. 19, no. 4, pp. 197–199, Apr. 2009.

[59] M. Durán-Sindreu, F. Aznar, A. Vélez, J. Bonache, and F. Martín, "Analysis and applications of OSRR- and OCSRR-loaded transmission lines: A new path for the design of compact transmission line metamaterials," *Metamaterials*, vol. 4, nos. 2–3, pp. 139–148, Aug. 2010.

[60] M. Makimoto and S. Yamashita, "Compact bandpass filters using stepped impedance resonators," *Proc. IEEE*, vol. 67, no. 1, pp. 16–19, Jan. 1979.

[61] M. Makimoto and S. Yamashita, "Bandpass filters using parallel coupled stripline stepped impedance resonators," *IEEE Trans. Microw. Theory Techn.*, vol. MTT-28, pp. 1413–1417, 1980.

[62] J. Naqui, M. Durán-Sindreu, J. Bonache, and F. Martín, "Implementation of shunt connected series resonators through stepped-impedance shunt stubs: Analysis and limitations," *IET Microw., Antennas Propag.*, vol. 5, pp. 1336–1342, Aug. 2011.

[63] D. M. Pozar, *Microwave Engineering*, 4th ed. Hoboken, NJ, USA: Wiley, 2011.

[64] G. Galindo-Romera, F. J. Herraiz-Martínez, M. Gil, J. J. Martínez-Martínez, and D. Segovia-Vargas, "Submersible printed split-ring resonator-based sensor for thin-film detection and permittivity characterization," *IEEE Sensors J.*, vol. 16, no. 10, pp. 3587–3596, May 2016.

[65] J. Muñoz-Enano, J. Martel, P. Vélez, F. Medina, L. Su, and F. Martín, "Parametric analysis of the edge capacitance of uniform slots and application to frequency-variation permittivity sensors," *Appl. Sci.*, vol. 11, no. 15, p. 7000, Jul. 2021.

[66] M. Abdolrazzaghi, M. Daneshmand, and A. K. Iyer, "Strongly enhanced sensitivity in planar microwave sensors based on metamaterial coupling," *IEEE Trans. Microw. Theory Techn.*, vol. 66, no. 4, pp. 1843–1855, Apr. 2018.

[67] M. Abdolrazzaghi and M. Daneshmand, "Exploiting sensitivity enhancement in micro-wave planar sensors using intermodulation products with phase noise analysis," *IEEE Trans. Circuits Syst. I, Reg. Papers*, vol. 67, no. 12, pp. 4382–4395, Dec. 2020.

[68] A. M. Albishi, M. K. E. Badawe, V. Nayyeri, and O. M. Ramahi, "Enhancing the sensitivity of dielectric sensors with multiple coupled complementary split-ring resonators," *IEEE Trans. Microw. Theory Techn.*, vol. 68, no. 10, pp. 4340–4347, Oct. 2020.

PAU CASACUBERTA was born in Sabadell (Barcelona), Spain, in 1997. He received the bachelor's degree in electronic telecommunications engineering and computer engineering from the Universitat Autònoma de Barcelona (UAB), in 2020, where he is currently pursuing the master's degree in telecommunications engineering. In 2019, he received the Collaboration Fellowship by the Spanish Government for developing his bachelor's thesis in highly sensitive microwave sensors-based in stepped impedance structures. He is currently working in the elaboration of his Ph.D. degree, which is focused on the development of microwave sensors for the characterization of the composition of multicomponent liquid substances with a research grant from FPU Program of the Universities Spanish Ministry.

PARIS VÉLEZ (Senior Member, IEEE) was born in Barcelona, Spain, in 1982. He received the bachelor's degree in telecommunications engineering, specializing in electronics, the master's degree in electronics engineering, and the Ph.D. degree in electrical engineering from the Universitat Autònoma de Barcelona, Spain, in 2008, 2010, and 2014, respectively. His Ph.D. thesis concerned common mode suppression differential microwave circuits based on metamaterial concepts and semi-lumped resonators. During the Ph.D. degree, he was awarded with a pre-doctoral teaching and research fellowship by the Spanish Government, from 2011 to 2014. From 2015 to 2017, he was involved in the subjects related to metamaterials sensors for fluidics detection and characterization at LAAS-CNRS through a TECNIOSpring Fellowship co-founded by the Marie Curie Program. From 2018 to 2020, he was worked in miniaturization of passive circuits RF/microwave and sensors-based metamaterials through Juan de la Cierva Fellowship. His current research interests include the miniaturization of passive circuits RF/microwave and sensors-based metamaterials. He is a Reviewer of the IEEE TRANSACTIONS ON MICROWAVE THEORY AND TECHNIQUES and for other journals.

JONATHAN MUÑOZ-ENANO (Graduate Student Member, IEEE) was born in Mollet del Vallès (Barcelona), Spain, in 1994. He received the bachelor's degree in electronic telecommunications engineering and the master's degree in telecommunications engineering from the Autonomous University of Barcelona (UAB), in 2016 and 2018, respectively. Actually, he is currently working with UAB in the elaboration of his Ph.D. degree, which is focused on the development of microwave sensors based on metamaterials concepts for the dielectric characterization of materials and biosensors.

LIJUAN SU (Member, IEEE) was born in Qianjiang (Hubei), China, in 1983. She received the B.S. degree in communication engineering and the M.S. degree in circuits and systems from the Wuhan University of Technology, Wuhan, China, in 2005 and 2013, respectively, and the Ph.D. degree in electronic engineering from the Universitat Autònoma de Barcelona, Barcelona, Spain, in 2017. From November 2017 to December 2019, she worked as a Postdoctoral Researcher with the Flexible Electronics Research Center, Huazhong University of Science and Technology, Wuhan. She is currently a Postdoctoral Researcher with CIMITEC, Universitat Autònoma de Barcelona. Her current research interests include the development of novel microwave sensors with improved performance for biosensors, dielectric characterization of solids and liquids, defect detection, and industrial processes.

MARTA GIL BARBA (Member, IEEE) was born in Valdepeñas, Ciudad Real, Spain, in 1981. She received the degree in physics from the Universidad de Granada, Spain, in 2005, and the Ph.D. degree in electronic engineering from the Universitat Autònoma de Barcelona, Barcelona, Spain, in 2009. She studied one year with Friedrich Schiller Universität Jena, Jena, Germany. During her Ph.D. thesis, she was a Holder of a METAMORPHOSE NoE Grant and National Research Fellowship from the FPU Program of the Education and Science Spanish Ministry. As a Postdoctoral Researcher, she was awarded with a Juan de la Cierva Fellowship working with the Universidad de Castilla-La Mancha. She was a Postdoctoral Researcher with the Institut für Mikrowellentechnik und Photonik, Technische Universität Darmstadt, and the Carlos III University of Madrid. She is currently an Associate Professor with the Universidad Politécnica de Madrid within the Excellence Program for University Professoriate of the V Regional Plan for Scientific Research and Technological Innovation (V PRICIT) of the Administration of the Community of Madrid. She has worked in metamaterials, piezoelectric MEMS, and microwave passive devices. Her current interest includes metamaterials sensors for fluidic detection.

AMIR EBRAHIMI (Member, IEEE) received the B.Sc. degree in electrical engineering, in 2008, the M.Sc. degree in microelectronics, in 2011, and the Ph.D. degree from The University of Adelaide, Adelaide, SA, Australia, in 2016.

From 2014 to 2015, he was a Visiting Research Fellow with Nanyang Technological University (NTU), Singapore. He is currently a Postdoctoral Researcher with the School of Engineering, RMIT University, Melbourne, VIC, Australia. His research interests include metamaterial inspired microwave devices, microwave circuit design, microwave filters, frequency-selective surfaces (FSSs) and nonlinear RF, and microwave circuits design and analysis. He was a recipient of the Australian National Fabrication Facility (ANFF) Award, in 2013, the University of Adelaide D. R. Stranks Traveling Fellowship, in 2014, the Yarman–Carlin Best Student Paper Award at the Mediterranean Microwave Symposium, in 2015, the Simon Rockliff Scholarship, in 2016, the Best Paper Award at the Australian Microwave Symposium, in 2016, Gertrude Rohan Memorial Prize, in 2017, and the CASS Foundation Travel Award, in 2019. He is a Reviewer for several recognized international journals, such as the IEEE Transactions on Microwave Theory and Techniques, the IEEE Transactions on Antennas and Propagations, and the IEEE Microwave and Wireless Components Letters.

FERRAN MARTÍN (Fellow, IEEE) was born in Barakaldo (Vizcaya), Spain, in 1965. He received the B.S. degree in physics from the Universitat Autònoma de Barcelona (UAB), in 1988, and the Ph.D. degree, in 1992.

From 1994 to 2006, he was an Associate Professor in electronics with the Departament d'Enginyeria Electrònica (Universitat Autònoma de Barcelona), and since 2007, he has been a Full Professor in electronics. In recent years, he has been involved in different research activities, including modeling and simulation of electron devices for high frequency applications, millimeter wave and THz generation systems, and the application of electromagnetic bandgaps to microwave and millimeter wave circuits. He is currently very active in the field of metamaterials and their application to the miniaturization and optimization of microwave circuits and antennas. He is currently the Head of the Microwave Engineering, Metamaterials and Antennas Group (GEMMA Group), UAB, and the Director of CIMITEC, a Research Center on Metamaterials supported by TECNIO (Generalitat de Catalunya). He has organized several international events related to metamaterials and related topics, including Workshops at the IEEE International Microwave Symposium, in 2005 and 2007, and European Microwave Conference, in 2009, 2015, and 2017, and the Fifth International Congress on Advanced Electromagnetic Materials in Microwaves and Optics (Metamaterials 2011), where he acted as the Chair of the Local Organizing Committee. He has acted as the Guest Editor for six Special Issues on metamaterials and sensors in five international journals. He has authored and coauthored over 650 technical conference, letter, journal articles, and book chapters. He is the coauthor of the book on Metamaterials entitled *Metamaterials with Negative Parameters: Theory, Design and Microwave Applications* (John Wiley & Sons Inc.), the author of the book *Artificial Transmission Lines for RF and Microwave Applications* (John Wiley & Sons Inc.), a Co-Editor of the book *Balanced Microwave Filters* (Wiley/IEEE Press), and the coauthor of the book *Time-Domain Signature Barcodes for Chipless-RFID and Sensing Applications* (Springer). He has generated 21 Ph.D.'s, has filed several patents on metamaterials and has headed several development contracts. His research interests include microwave sensors and RFID systems, with special emphasis on the development of high data capacity chipless-RFID tags. He is a member of the IEEE Microwave Theory and Techniques Society (IEEE MTT-S). He is a Reviewer of the IEEE Transactions on Microwave Theory and Techniques and IEEE Microwave and Wireless Components Letters, and among many other journals. He serves as a member for the Editorial Board of *IET Microwaves, Antennas and Propagation*, *International Journal of RF and Microwave Computer-Aided Engineering*, and *Sensors*. He was a recipient of three ICREA ACADEMIA Awards (calls 2008, 2013, and 2018). He is a fellow of the IET. He is also a member of the Technical Committees of the European Microwave Conference (EuMC) and International Congress on Advanced Electromagnetic Materials in Microwaves and Optics (Metamaterials). Among his distinctions, he has received the 2006 Duran Farell Prize for Technological Research, he holds the Parc de Recerca UAB—Santander Technology Transfer Chair.